A Monte Carlo dosimetry-based evaluation of the ^{7}Li(p,n)^{7}Be reaction near threshold for accelerator boron neutron capture therapy

C. L. Lee[a] and X.-L. Zhou
Department of Nuclear Engineering, Massachusetts Institute of Technology, Cambridge, Massachusetts 02139

R. J. Kudchadker and F. Harmon
Department of Physics, Idaho State University, Pocatello, Idaho 83209

Y. D. Harker
Idaho National Engineering and Environmental Laboratory, Idaho Falls, Idaho 83415

(Received 5 April 1999; accepted for publication 18 October 1999)

Advanced methods of boron neutron capture therapy (BNCT) use an epithermal neutron beam in conjunction with tumor-targeting boron compounds for irradiation of glioblastomas and metastatic melanomas. A common neutron-producing reaction considered for accelerator-based BNCT is ^{7}Li(p,n)^{7}Be, whose cross section increases very rapidly within several tens of keV of the reaction threshold at 1.88 MeV. Operation in the proton energy region near threshold will have an appreciable thick target neutron yield, but the neutrons produced will have relatively low energies that require little moderation to reach the epithermal range desirable for BNCT. Because of its relatively low projected accelerator cost and the portability of the neutron source/target assembly, BNCT based on the near-threshold technique is considered an attractive candidate for widespread hospital use. A systematic Monte Carlo N-Particle (MCNP) investigation of the dosimetric properties of near-threshold neutron beams has been performed. Results of these studies indicate that accelerator proton energies between 1.93 and 1.99 MeV, using 5 cm of H_2O moderator followed by thin ^{6}Li and Pb shields, can provide therapeutically useful beams with treatment times less than one hour and accelerator currents less than 5 mA. © *2000 American Association of Physicists in Medicine.* [S0094-2405(00)03101-1]

Key words: epithermal neutrons, accelerator, neutron capture therapy, near threshold

I. INTRODUCTION

Boron neutron capture therapy (BNCT), a binary treatment modality that is primarily studied for the treatment of glioblastoma tumors, achieves high doses to the target region of the brain by injecting a boronated compound into the patient, followed by irradiation with an epithermal neutron beam. The boron compound, which preferentially accumulates in cancerous cells, provides highly localized dose deposition in the tumor due to the energetic heavy charged particles from the ^{10}B(n,α)^{7}Li reaction. The lower boron accumulation in surrounding healthy tissue results in relative sparing of these tissues.[1] Additional potential applications of the BNCT concept include treatment of peripheral and intracranial metastatic melanomas, as well as rheumatoid arthritis.[2,3]

BNCT research in the United States and Europe is concentrated on the use of epithermal neutron beams. An epithermal beam produces a peak in the thermal neutron flux, and hence boron neutron capture rate, at a distance several centimeters below the skin surface. This permits deeply seated tumors to be treated without excessively high doses to the scalp. In addition, the removal of the skull cap during irradiation, which is required for irradiations with thermal neutron beams, is unnecessary with more penetrating epithermal neutron beams. Previous work has established that the range of epithermal neutron energies ideal for BNCT is $\sim$1 eV to $\sim$10 keV.[4]

Accelerator neutron sources, considered necessary for the successful implementation of BNCT in hospital settings, must provide intense (to permit reasonable treatment times) epithermal beams with small fast neutron, thermal neutron, and γ-ray contamination. The reaction most commonly studied for neutron sources in accelerator-based BNCT research is ^{7}Li(p,n)^{7}Be, since the rapid increase in the reaction cross section at proton energies just above threshold provides a significant source of relatively low energy neutrons. For example, the (p,n) cross section reaches 270 mb within only 50 keV of 1.88 MeV, the reaction threshold energy,[5] and the resulting thick target neutron yield is 2.58×10^{12} neutrons/mA-min. In addition, since the maximum and mean neutron energies for this source are 137 keV and 50.6 keV, only a small amount of moderation is required to reach the epithermal energy range defined above.

Other researchers have concentrated on simulations using proton bombarding energies around 2.5 MeV in order to take advantage of the 2.25 MeV resonance where the (p,n) cross section is 580 mb.[6–8] This proton bombarding energy produces large neutron yields as the beam slows down in the thick lithium target (5.30×10^{13} neutrons/mA-min). However, the maximum and mean neutron energies are 787 keV and 326 keV, respectively, and therefore they require extensive moderation to reduce the neutron energies to the epithermal region. It is possible that the lower neutron energies

produced with proton energies near the reaction threshold will offset the higher intensity produced with a 2.5 MeV bombarding energy, and that a more efficient moderator system can be designed. This approach has led to the development of near-threshold BNCT as a potential alternative to common accelerator-based BNCT methods.[9–11]

Previous work has studied near-threshold beams based on in-air figures of merit, such as useful neutron flux, current-to-flux ratio, and ratios of fast neutron and photon dose rate to useful neutron flux.[12] These figures of merit are often used to describe and compare reactor neutron beams for BNCT.[13,14] However, these in-air parameters present an incomplete picture, since patient dosimetry is not included in the evaluation.

A systematic study of near-threshold neutron beams based on calculations of patient dosimetry using a cylindrical head phantom has been performed as part of this work. Dose rates have been calculated for fast neutrons (mainly due to elastic scattering of hydrogen), thermal neutrons (mainly due to the proton and carbon nucleus recoils from the $^{14}N(n,p)^{14}C$ reaction), photons (mainly due to 2.22 MeV γ-rays from thermal neutron capture by hydrogen), and tumor and healthy tissue boron (from high linear energy transfer α particles and ^{7}Li ions). These dose rates have been used to estimate treatment time, beam penetrability, and therapeutic effectiveness using a dosimetric set of BNCT figures of merit (described below). These results have been used to design a unified target/moderator/reflector assembly that is applicable to hospital-based treatment of glioblastomas using BNCT.

II. BNCT TREATMENT FIGURES OF MERIT

Three quantities, initially defined by Zamenhof et al.,[15] are used in this work to provide quantitative descriptions of the therapeutic efficacy of neutron beams for BNCT: (1) advantage depth (AD), which indicates the penetrability of the neutron beam; (2) advantage ratio (AR), which gives the tumor dose relative to surrounding healthy tissue dose; and (3) advantage depth dose rate (ADDR), an indicator of treatment time.

The advantage depth is defined as the depth in a phantom at which point the tumor dose rate equals the maximum healthy tissue dose rate. Any tumor mass located beyond the AD receives less than the maximum healthy tissue dose, thus reducing any treatment ''advantage.'' The advantage ratio is defined as the ratio of the areas under the dose rate curves for tumor and healthy tissue along the phantom centerline from the surface to the advantage depth:

$$\mathrm{AR}=\frac{\int_0^{\mathrm{AD}} D_{\mathrm{tumor}}(z)\,dz}{\int_0^{\mathrm{AD}} D_{\mathrm{tissue}}(z)\,dz}, \tag{1}$$

where $D_{\mathrm{tumor}}(z)$ and $D_{\mathrm{tissue}}(z)$ are the doses to tumor and healthy tissue, respectively, along the centerline (z-axis) of the phantom. Finally, the advantage depth dose rate is defined as the tumor dose rate at the advantage depth, which is equal to the maximum healthy tissue dose rate. Since the total dose to healthy tissue is usually a limiting factor for treatments, the ADDR determines the treatment time for the patient (treatment time=allowed healthy tissue dose/maximum healthy tissue dose rate). The units of AD are cm, the units of the ADDR are cGy/mA-min, and the AR is dimensionless. It is desirable to have all three parameters as large as possible for a well-designed beam.

In all dosimetry calculations of biological systems, dose components should be weighted with appropriate relative biological effectiveness (RBE) factors. The following RBE values are used for the dose components in these BNCT simulations: fast neutron, 3.2; thermal neutron, 3.2; ^{10}B in healthy tissue, 1.35; ^{10}B in tumor, 3.8; photon, 1.0. Currently, these RBE values are being used in clinical BNCT trials at the Massachusetts Institute of Technology (MIT) and Brookhaven National Laboratory (BNL).[16,17] In these trials, the pharmaceutical boronophenylalanine (BPA) is the boron delivery compound. Using BPA, the tumor-to-healthy tissue uptake ratio of ^{10}B is 3.5 and the tumor uptake concentration is 40 μg ^{10}B/g tissue, or 40 ppm. Any adjustment of these RBE values will change all three figures of merit defined above, and intercomparisons of the results presented here with published results for other neutron beams must take this into account. It should be noted that tumor and healthy tissue boron RBE values are unlikely to differ between reactor and near-threshold beams, since they are primarily determined by the distribution of the boron compound within cells. However, the neutron RBE values for near-threshold beams may differ appreciably from those for reactor beams, because the neutron energy spectra of reactor and near-threshold beams differ. Since RBE values for near-threshold neutron energy spectra of have not been determined, the RBE values given above are considered at this point a ''best guess'' and are used for comparison purposes only.

In most cases, an adjustment to a neutron beam that improves one of these treatment parameters has a detrimental effect on one or both of the other parameters. Since high values are desirable for all three parameters, a compromise is necessary in choosing the target/moderator/reflector combination (hereafter called the combined target unit, or CTU). This also means that no particular neutron beam is clearly ''optimum,'' and the design of the CTU is thus driven by minimally acceptable requirements on treatment parameters such as treatment time and penetration depth. These in turn dictate minimally acceptable values for the RBE-weighted AD (RBE-AD) and ADDR (RBE-ADDR), respectively. Near-threshold designs that produce RBE-AD and RBE-ADDR values exceeding these minimum requirements form an envelope of acceptable solutions. In establishing a basis for the design of a CTU, the following parameters were used to define the acceptability envelope for treatment:

- RBE-AD$>$5 cm
- Maximum healthy brain dose $<$12.5 RBE-Gy
- Nominal accelerator current $<$5 mA
- Treatment time $<$1 hour
- RBE-ADDR$>$4.2 RBE-cGy/mA-min

Treatment plans for the BNL clinical trials have used a

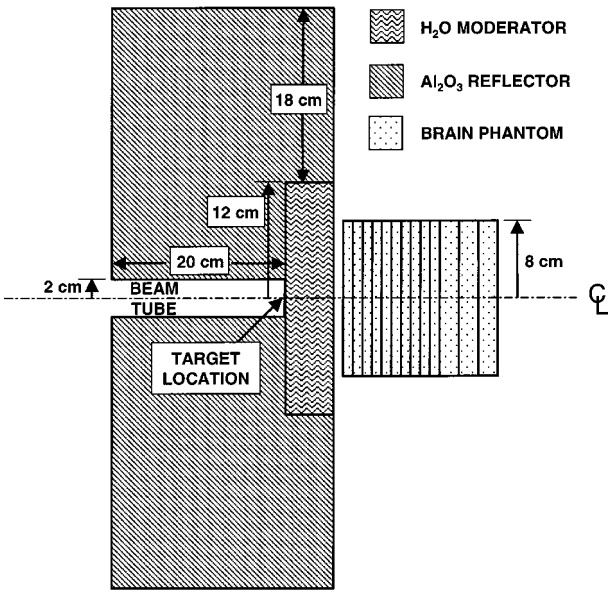

FIG. 1. Geometry of MCNP model used for near-threshold BNCT studies. All components have cylindrical symmetry. This configuration has a 5 cm thick light water (H_2O) moderator with an alumina (Al_2O_3) reflector.

maximum healthy brain tissue dose of 12.5 RBE-Gy. The nominal accelerator current is close to the lowest accelerator current (4 mA) for accelerator-based BNCT beam designs found in current literature.[7] A maximum treatment time of 1 hour should provide sufficient patient throughput to make this treatment economically viable for hospital use. Dividing the maximum healthy tissue dose by the nominal accelerator current and the maximum treatment time gives a target value of 4.2 RBE-cGy/mA-min for the RBE-ADDR.

III. MCNP INPUT DESCRIPTION

The radiation transport necessary to calculate the BNCT figures of merit described in Sec. II was performed using the Monte Carlo N-Particle (MCNP) radiation transport computer program.[18] The basic MCNP geometry for a moderator thickness of 5 cm is given in Fig. 1. There is cylindrical symmetry for all objects shown. In the simplest MCNP runs, only the beam tube, moderator, reflector, and phantom were modeled. The lithium target was not included in the model since it has dimensions on the order of tens of microns (see Sec. IV below). The moderator thickness was variable in these studies. The outer edge of the reflector was adjusted in each calculation to keep it flush with the outer surface of the moderator. All other dimensions were invariant. In later calculations, additional sheets of material were added to the outer face of the moderator (see Secs. V B and V C below) to suppress thermal neutron and photon contamination. The phantom was located 1 cm from the outer surface of the CTU. The 16 cm long phantom was divided into thirteen disks in order to tally fluxes and doses as a function of depth into the phantom. Concentric cylindrical shells were also defined to determine the radial variation of all fluxes and doses.

The neutron source definition for the MCNP input deck was of uniform intensity (in source neutrons/cm^2) within a 1 cm radius circular region at the target end of the beam tube. The neutron energy spectrum was given as a histogram distribution with 10 keV-wide intervals. For each energy bin, the angular distribution of neutrons was represented by 10°-wide angle histograms. The doubly differential thick target neutron yields were calculated using a program written to provide accurate neutron yields for near-threshold protons on lithium targets.[19] While BNCT was the motivation for developing this computer program, it may be used to predict neutron angular distributions and energy spectra for any proton energy below 3 MeV in a wide variety of accelerator applications that use the ^{7}Li$(p,n)^7$Be reaction. The neutron yields predicted by this program have been experimentally benchmarked for lithium, lithium fluoride, and lithium oxide targets.[20]

The beam tube was modeled as vacuum, while the moderator and reflector were light water (H_2O) and aluminum oxide (Al_2O_3), respectively. These materials have been shown previously to be ideal candidates for near-threshold BNCT.[12] The phantom was made of brain-equivalent material consisting of a 50/50 combination of white and grey brain matter by weight. The brain density and material composition were taken from Brooks *et al.*[21]

The neutron flux tallied in each of the phantom cells was converted to a physical dose rate using total neutron target yields (in neutrons/mA-min) and fluence-KERMA values for fast neutron, thermal neutron, and ^{10}B doses. Two important details permit the absorbed dose rates of these components to be approximated by the corresponding KERMA rates: charged particle equilibrium exists to a good approximation (except within the very small distance from the phantom surface equal to the maximum range of the heavy secondary charged particles), and bremsstrahlung production by these heavy secondary charged particles is negligible. The neutron KERMA values were taken from tabulated values from Caswell *et al.*,[22] while the ^{10}B KERMA values were those determined by Zamenhof *et al.*[15] The photon dose was calculated using photon heating tallies provided by MCNP. One million source neutrons were used in all calculations to produce doses with relative errors less than 5% for all depths in the phantom.

IV. PHOTONS PRODUCED IN THE LITHIUM TARGET

While neutrons are the most important BNCT source component from a lithium target, photons are also produced. These include 478 keV gammas from inelastic proton scattering $(p,p'\gamma)$ and 14 to 18 MeV gammas from radiative capture (p,γ). As will be shown below, these dose components can have a serious impact on the total dose and the therapeutic parameters defined in Sec. II.

Tabulated thick target photon yields for inelastic proton scattering in the lithium target have been published by Kiss.[23] A least squares quadratic fit to Kiss' data is given by the equation

$$\sqrt{Y_{p-p'\gamma}} = 2.658\times 10^6 E_p - 1.933\times 10^6, \quad (2)$$

TABLE I. A comparison of neutron and photon yields for thick natural lithium targets.

Incident proton energy (MeV)	Neutron yield (N/mA min)	478 keV gamma yield (γ/mA min)	Gamma yield relative to neutron yield
1.89	3.80×10^{11}	9.54×10^{12}	25.10
1.90	8.94×10^{11}	9.72×10^{12}	10.90
1.91	1.45×10^{12}	9.90×10^{12}	6.84
1.92	2.01×10^{12}	1.01×10^{13}	5.00
1.93	2.58×10^{12}	1.02×10^{13}	3.96
1.94	3.15×10^{12}	1.04×10^{13}	3.30
1.95	3.73×10^{12}	1.06×10^{13}	2.84
1.96	4.30×10^{12}	1.07×10^{13}	2.50
1.97	4.87×10^{12}	1.09×10^{13}	2.24
1.98	5.45×10^{12}	1.11×10^{13}	2.04
1.99	6.00×10^{12}	1.13×10^{13}	1.88
2.00	6.60×10^{12}	1.15×10^{13}	1.74
2.10	1.28×10^{13}	1.33×10^{13}	1.04
2.20	2.17×10^{13}	1.54×10^{13}	0.706
2.30	3.47×10^{13}	1.75×10^{13}	0.504
2.40	4.67×10^{13}	1.98×10^{13}	0.424
2.50	5.30×10^{13}	2.22×10^{13}	0.419

TABLE II. Reduced target thicknesses for natural lithium metal. These thicknesses are sufficient to reduce the mean energy of a proton beam from the incident value to 1.88 MeV, the ^{7}Li$(p,n)^7$Be reaction threshold.

Incident proton energy (MeV)	Lithium target thickness (μm)
1.89	1.33
1.90	2.67
1.91	4.01
1.92	5.36
1.93	6.71
1.94	8.07
1.95	9.43
1.96	10.8
1.97	12.2
1.98	13.6
1.99	14.9
2.00	16.3
2.10	30.6
2.20	45.5
2.30	60.8
2.40	76.7
2.50	93.1

where $Y_{p-p'\gamma}$ is the 478 keV photon yield in photons/mA-min and E_p is the incident proton energy in MeV. Table I gives a comparison of neutron and photon yields for thick lithium targets. It is clear that for near-threshold energies, the gamma yield from inelastic proton scattering in the target completely dominates the neutron yield. The effect of these photons on the BNCT treatment parameters for a 1.93 MeV proton beam with 3 cm of water moderator is shown in Fig. 2. The two curves with open symbols correspond to results in which the 478 keV gammas are ignored. The neutron beam appears to have an RBE-AD of 4.4 cm, an RBE-AR of 4.3, and an RBE-ADDR of 29 RBE-cGy/mA-min. The two curves with solid symbols include the effects of the inelastic proton scattering gammas. These doses are calculated in a separate photon-only MCNP run with an isotropic, 478 keV photon source having a total yield given by Eq. (2). The total photon dose in the phantom is the sum of the doses from both MCNP runs. The RBE-ADDR increases dramatically, but the RBE-AD drops to only 2.5 cm, with a similar drop of the RBE-AR to 2.2.

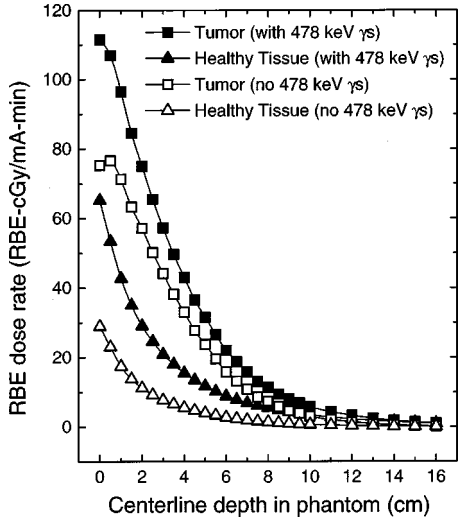

FIG. 2. Variation of centerline RBE dose with depth. Curves with solid symbols include the effects of gamma-rays produced from inelastic proton scattering in the lithium target, while curves with open symbols do not.

The scenario above assumes a thick target where the proton beam is stopped in the lithium. It appears from this model that the near-threshold approach to BNCT is not feasible. However, neutrons are only produced in lithium for proton energies above 1.88 MeV, and 478 keV inelastic scatter gammas are produced for proton energies down to 550 keV. If the lithium target is made just thick enough to slow the proton beam past the (p,n) threshold of 1.88 MeV, there is no loss of neutron yield, but the inelastic scatter gamma yield is reduced significantly. The reduced target thickness can be constructed by vapor deposition of lithium or a lithium compound directly onto a backing material. Lithium target thicknesses required to slow the protons to 1.88 MeV are given in Table II. They are calculated by integrating the inverse of tabulated stopping powers over proton energy.[24] The remaining proton energy deposition will occur in the target backing material, which can be chosen to limit production of significant gammas from similar reactions. The reduced gamma yield for incident proton energy E_p, denoted $Y^*_{p-p'\gamma}(E_p)$, is given by the difference $Y^*_{p-p'\gamma}(E_p) = Y_{p-p'\gamma}(E_p) - Y_{p-p'\gamma}(E_{th})$.

The reduced target thickness concept reduces the gamma yield to levels that allow near-threshold treatment beams to again be feasible, although the 478 keV gamma source is still a significant effect and must always be taken into account. All MCNP calculations reported in this work include the dose due to the photons from inelastic proton scattering in the reduced thickness lithium target. The reduced thickness lithium target has additional advantages as far as solving the target heat removal problem. However, there are concerns

regarding target stability and lifetime due to differential thermal expansion of target and backing materials.[25]

The photon yield from the (p,γ) reaction may be estimated from the thick target formula

$$Y_{p-\gamma}=N_{\mathrm{Li}-7}\int_0^{E_{p_0}}\frac{\sigma_{p-\gamma}(E_p)}{-\dfrac{dE_p}{dx}}\,dE_p, \tag{3}$$

where $Y_{p-\gamma}$ is the total photon yield due to the (p,γ) reaction in lithium, $N_{\mathrm{Li}-7}$ is the number density of ^{7}Li atoms in the target, E_{p0} is the incident proton energy, $\sigma_{p-\gamma}(E_p)$ is the total (p,γ) cross section as a function of proton energy E_p, and $-dE_p/dx$ is the proton stopping power in lithium metal. Using the (p,γ) cross section, which has a large, narrow resonance at 411 keV,[26] and tabulated proton stopping powers in lithium,[24] the calculated thick target (p,γ) gamma yield is 3.37×10^8 photons/mA-min for 1.95 MeV proton beams. Because the vast majority of photons are produced by the 411 keV resonance, there is less than 1% difference in (p,γ) photon yields for other incident proton energies. This yield is at least three orders of magnitude lower than the other yields given in Table I and is neglected in all subsequent dose calculations.

V. DOSE CALCULATIONS

A systematic study of the effects of proton beam energy (between 1.89 MeV and 1.99 MeV) and light water moderator thickness (from 1 cm to 9 cm) on RBE-weighted advantage depth, advantage ratio, and advantage depth dose rate was performed for near-threshold neutron beams. In addition, the effects of thermal neutron attenuation (^{6}Li), photon shielding (Pb), and structures related to target cooling (Cu) on these advantage parameters were evaluated.

As mentioned in Sec. III, H_2O has been shown in a previous study to be an effective moderator for near-threshold beams,[12] although this is not true for neutron sources produced with higher energy protons. This difference is due to the lower neutron energies produced by near-threshold protons: they require small amounts of moderation to reduce the fast neutron component to an acceptable level, and a useful treatment beam can be obtained before the thermal neutron beam component (and accompanying 2.2 MeV hydrogen capture gamma component) builds up to an unacceptably high level. For higher proton energies, however, the amount of H_2O necessary to reduce the fast neutron component is much greater, and the thermal neutron and capture gamma fluxes that arise are unacceptably large. In addition, the H_2O moderator may serve as the target coolant.

Other parameters, which remained constant in all computations, included proton beam spot size (1 cm radius); reflector material (Al_2O_3) and inner and outer radii (12 cm and 30 cm, respectively); moderator radius (12 cm); distance from moderator face to phantom face (1 cm); and phantom shape (cylindrical) and size (8 cm radius, 16 cm length). Because the effects of varying these parameters on beam performance have been previously studied,[27,28] these parameters were not varied in this work.

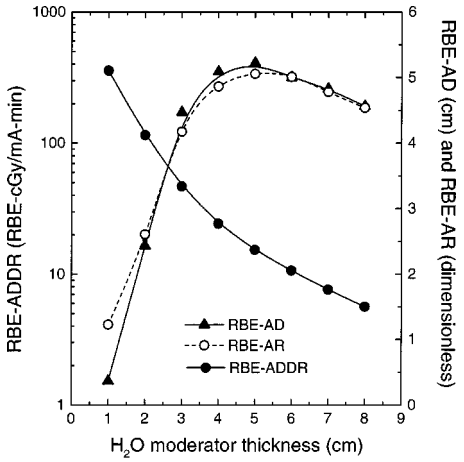

FIG. 3. Variation of RBE-weighted advantage depth (RBE-AD), advantage ratio (RBE-AR), and advantage depth dose rate (RBE-ADDR) with moderator thickness for neutrons produced with 1.95 MeV proton beams. RBE values are given in Sec. II.

A. Moderator effects

The primary parameters, related to moderation, that influence the treatment parameters are proton beam energy and moderator thickness. These parameters were the first to be varied in the basic CTU configuration study. The variation of RBE-AD, RBE-AR, and RBE-ADDR as functions of moderator thickness for a representative proton beam energy of 1.93 MeV are given in Fig. 3. The RBE-AD and RBE-AR increase rapidly for moderator thicknesses less than 3.5 cm, then reach a peak at between 5 and 6 cm of water and slowly decrease, while the RBE-ADDR decreases monotonically with moderator thickness.

The variation of RBE-AD with moderator thickness for multiple proton energies is shown in Fig. 4, while Fig. 5 provides the RBE-ADDR variations. For all data points in Fig. 4, error propagation calculations produce absolute sta-

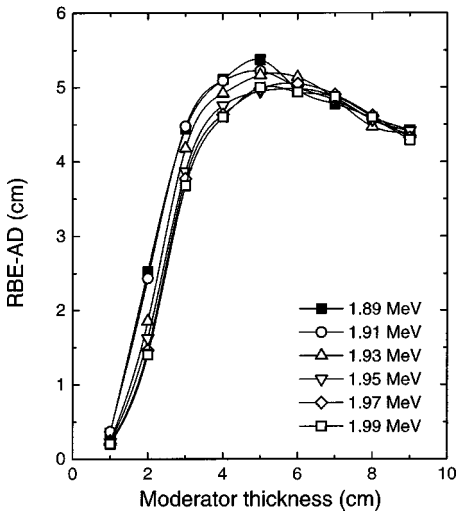

FIG. 4. Variation of advantage depth (AD) with moderator thickness for near-threshold neutron beams. The advantage depths are calculated using RBE-weighted doses.

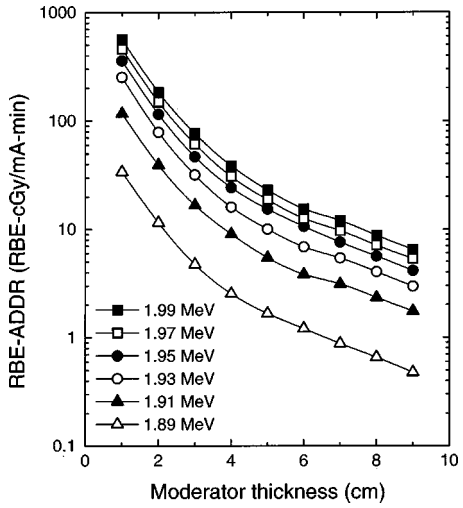

FIG. 5. Variation of advantage depth dose rate (ADDR) with moderator thickness for near-threshold neutron beams. The advantage depth dose rates are calculated using RBE-weighted doses.

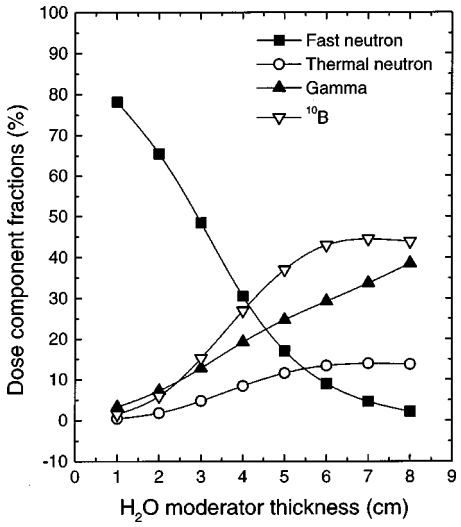

FIG. 6. Percentages of healthy tissue RBE-weighted dose components on the front face of a phantom for a neutron beam produced using a 1.95 MeV proton beam.

tistical errors in the RBE-AD of less than 0.15 cm, and relative errors in the RBE-ADDR under 5%. For all near-threshold energies, the RBE-AD has a rapid initial increase due to the reduction of the fast neutron dose component, reaches a peak around 5–6 cm, and slowly decreases for larger amounts of moderator. It is clear from the data that there is little or no difference in near-threshold beams for moderator thicknesses above ~ 5 cm. The RBE-ADDR in Fig. 5 is seen to be highest for the highest proton beam energies, since the neutron yield increases with incident proton energy.

The results given in Figs. 3–5 include degrading effects due to fast neutron, thermal neutron, and γ contamination of the epithermal neutron beam. To improve on these results it is necessary to understand the contribution of each contamination component on the front face of the phantom. Therefore, additions and modifications to the basic design of the CTU can focus on reducing each particular beam contaminant in order to improve parameters such as advantage depth. Using the 1.95 MeV proton beam as a representative example, a plot of the variation of the dose percentage of these components, as well as the healthy tissue ^{10}B dose, with moderator thickness is given in Fig. 6. The fast neutron dose completely dominates for thinner moderators; this is expected, since there is not enough moderator to substantially reduce the neutron energies (and corresponding high KERMA values) in the beam. Since the fast neutron dose affects both tumor and healthy tissue equally, the advantage depth and advantage ratio are reduced. As the moderator thickness increases, the fast component quickly drops (and the RBE-AD and RBE-AR improve), while the other beam components slowly increase. Since thicker moderators produce larger thermal neutron fluxes, the external gamma dose due to photons from the $^1\mathrm{H}(n,\gamma)^2\mathrm{H}$ reaction will continuously increase with moderator thickness. As with fast neutrons, the gamma dose affects tumor and healthy tissue equally, so a point is reached where this dose component begins to erode all the gains made in the RBE-AD and RBE-AR by reducing the fast neutron component. The decrease in the RBE-AD due to an increase in γ contamination is not as dramatic as the rapid rise in the RBE-AD for low moderator thickness because the fast neutron RBE is more than three times the photon RBE.

Figure 6 also helps explain why there is little difference in the RBE-AD for near-threshold beams produced with different near-threshold proton energies for moderator thicknesses greater than ~ 5 cm. The neutron beams for all near-threshold proton energies become overmoderated with large H_2O thicknesses, consisting primarily of thermal neutrons and external gammas with a greatly reduced fast neutron component. The neutron beams essentially become thermal neutron beams with a significant gamma component, and any distinction between one near-threshold source neutron energy spectrum and another disappears. Both tumor and healthy tissue depth dose profiles are then primarily determined from thermal neutron, ^{10}B, and gamma doses, and the RBE-AD becomes nearly independent of proton energy.

Figures 4 and 5 are useful for seeing how the BNCT treatment parameters vary with moderator thickness, but it is difficult to see how they vary in unison for different CTU configurations. The plot in Fig. 7 facilitates this comparison by plotting the RBE-AD versus RBE-ADDR for each moderator thickness studied for a 1.95 MeV proton beam. As the moderator thickness increases, the RBE-AD (horizontal axis) increases and the RBE-ADDR (vertical axis) decreases until the maximum RBE-AD is reached at about 5 cm moderator thickness. The RBE-AD will then decrease (and hence bend back to the left) while the RBE-ADDR continues to decrease. All near-threshold beams have similar shapes.

The minimum acceptable RBE-AD and RBE-ADDR are plotted as dotted lines in Fig. 7. Any points located in the upper quadrant above and to the right of these lines meet the minimum requirements outlined in Sec. II. Proton energies

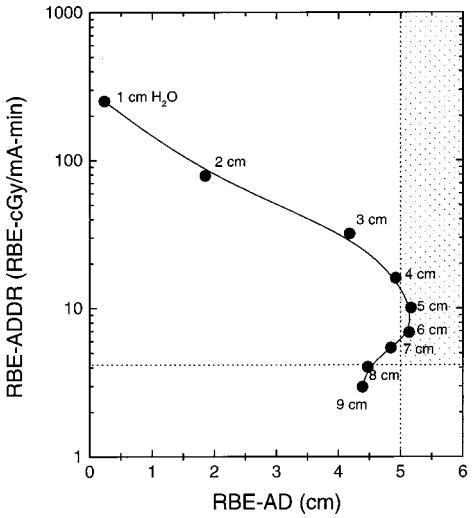

FIG. 7. Variation of RBE-weighted advantage depth (RBE-AD) and advantage depth dose rate (RBE-ADDR) as functions of moderator thickness for a neutron beam produced using a 1.95 MeV proton beam. Points above and to the right of the vertical and horizontal dotted lines satisfy the acceptability criteria discussed in Sec. II. Other near-threshold beams produce similar curves.

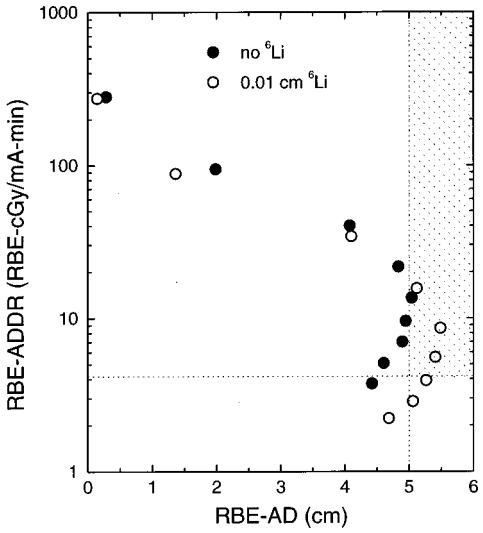

FIG. 8. Effect of a ^{6}Li thermal shield on RBE-weighted BNCT figures of merit for neutron beams produced using a 1.95 MeV proton beam and moderator thicknesses ranging from 1 to 9 cm.

from 1.91 to 1.97 MeV were found to produce RBE-AD versus RBE-ADDR curves with portions in this region. For proton energies less than 1.91 MeV, the neutron yields are too low to meet the minimum RBE-ADDR requirement. For proton energies greater than 1.97 MeV, the fast neutron and gamma doses are too large for thin and thick moderators, respectively, to meet the minimum RBE-AD requirement.

B. Thermal neutron attenuation

In an effort to reduce the thermal neutron component and thus improve the RBE-AD and RBE-AR of the beams under consideration, a thin (0.01 cm) sheet of ^{6}Li was placed on the downstream side of the moderator, between the moderator and phantom. This thickness of ^{6}Li will reduce the thermal neutron flux exiting the CTU by 31%. A 0.25 cm copper target backing was included in the calculations (see Sec. V D). Figure 8 shows the effects on the RBE-AD for a 1.95 MeV proton beam. The penetrability of the beam is seen to increase with the addition of ^{6}Li, as expected, but with a complementary decrease in the RBE-ADDR.

Cadmium is not a viable attenuator material, despite a larger thermal neutron absorption cross section than ^{6}Li, due to the large number of thermal neutron capture gammas that it produces. These gammas overwhelm any advantage that is gained by the reduction of the thermal neutron flux, actually reducing the RBE-AD rather than improving it. In the case of ^{6}Li, however, there is no gamma production, so the RBE-AD improves.

C. Photon attenuation

There is always an unavoidable gamma dose in the head due to hydrogen capture photons; nevertheless, any additional photon dose from the CTU degrades the effectiveness of the beam and should be reduced. Reduction of this external photon dose using lead sheets placed on the downstream side of the moderator and thermal neutron shield, between the other CTU components and the phantom, is a way to improve the RBE-AD and RBE-AR of these beams.

Several thicknesses of lead were placed on the downstream side of the moderator to gauge the effect of gamma attenuation on the BNCT treatment parameters. As with the thermal neutron shields described in Sec. V B, a 0.25 cm copper backing was included in all MCNP calculations. For each thickness of lead, the BNCT treatment parameters were calculated for the entire range of moderator thickness from 1 to 9 cm of H_2O in order to determine the water moderator thickness that gave the maximum RBE-AD for a given lead thickness. This moderator thickness was found to always be in the range from 5 to 6 cm.

The gains in the BNCT treatment parameters due to a thermal neutron shield, using ^{6}Li, and a photon shield, using lead, are shown in Fig. 9. In this figure, RBE-AD and RBE-ADDR are plotted for 1.95 MeV protons with no shielding, 0.01 cm of ^{6}Li shielding, and 0.25 cm of lead shielding. The ^{6}Li thermal neutron shield (open circles) leads to larger advantage depths, but the lead shield (solid triangles) gives higher advantage depth dose rates within the acceptability region. The combination of thermal neutron and photon shielding (open diamonds) is better still, with a maximum RBE-AD of nearly 6 cm.

D. Target cooling

The low melting point (181 °C) of lithium metal makes target cooling an important concern in any accelerator-based BNCT neutron beam design. This includes near-threshold beams, despite their lower proton energies. For example, a 5 mA beam of 1.95 MeV protons will deposit 9.75 kW of heat within the beam area, which in these calculations is a 2 cm diameter spot. While an entire paper is necessary to give a

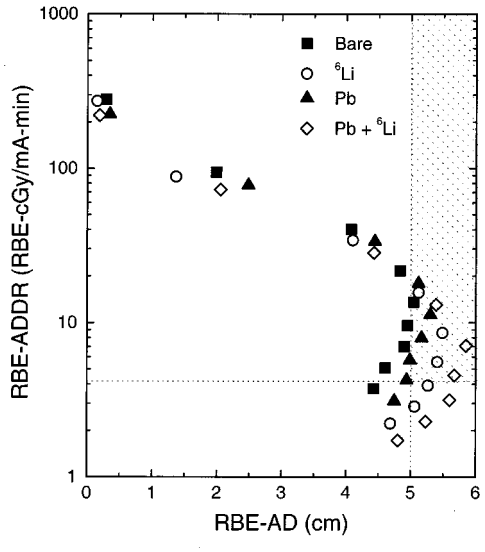

FIG. 9. Effect of ^{6}Li and Pb on RBE-weighted BNCT figures of merit for neutron beams produced using a 1.95 MeV proton beam. A combination of thermal neutron (^{6}Li) and photon (Pb) shields is seen to produce superior penetrability (RBE-AD) than with either shield alone.

full description of a cooling system for near-threshold neutron beams, some comments about target cooling and its effect on neutron transport are in order.

For a reduced thickness lithium target (see Sec. IV), the Bragg peak of the protons, as well as the majority of heat deposition, will be located in the target backing. A copper target backing was considered due to its high thermal conductivity and insignificant effect on advantage parameters.[29] Using tabulated proton stopping powers in lithium and copper,[24] the total temperature drop across target and backing has been calculated for 2.54 cm diameter beam spots with proton energies between 1.89 MeV and 2.5 MeV.[25] For a 9.5 μm thick Li target and 0.25 cm thick copper backing, the total temperature drop per unit proton current for a 1.95 MeV beam is 23.9 °C/mA. This temperature drop may be reduced by using a thinner target backing: reducing the copper thickness to 0.1 cm will decrease the total temperature drop across target and backing to 9.5 °C/mA. Note that the associated temperature drops for 2 cm diameter beam spots will be $1.27^2 = 1.6129$ times higher than those given above.

A prototypical target cooling configuration, which uses multiple rectangular copper fins protruding from the rear of the copper backing, has been studied elsewhere.[29] Fins are commonly used to increase the heat transfer surface area of a cooling surface. Using several fins spreads this improved heat transfer uniformly over the rear surface of the copper. In addition, multiple fins define coolant flow channels that create turbulence in the H_2O coolant stream, which further improves the heat transfer between copper and coolant.

For a ten gallon per minute (37.9 liters per minute) coolant flow rate of 20 °C light water, the temperature drop between the back surface of the copper disk and the bulk coolant was determined from calculation and experiment to be 17.6 °C/kW for this multi-fin cooling configuration. This gives a total temperature drop of 58.2 °C/mA between the lithium target surface and bulk coolant for a 1.95 MeV near-threshold proton beam with a 0.25 cm copper backing, or a total temperature drop of 43.9 °C/mA for a 0.1 cm copper backing. Additional temperature drops due to the duty factor and repetition rate of the particular accelerator being used must also be included.[30] For a 10% duty factor and 200 Hz repetition rate, the additional temperature drop for this configuration is estimated to be 3.0 °C/mA. For this cooling configuration, a safety margin of 40 °C for the peak lithium target temperature permits proton currents of 2.0 and 2.6 mA for 0.25 and 0.1 cm Cu backings, respectively. However, the temperature drop across target, backing, and coolant may be reduced by decreasing the bulk coolant entrance temperature, increasing the flow rate, changing the geometry of the cooling fins, increasing the area of the beam spot, or adjusting the duty factor and repetition rate of the accelerator. For example, increasing the beam spot radius from 1.0 cm to 1.5 cm increases the allowable proton currents to 4.4 and 5.8 mA for 0.25 and 0.1 cm Cu backings, respectively, without reducing the 40 °C safety margin for the peak lithium temperature.

The simplicity of the target cooling design using multiple fins does not appreciably change the overall CTU design from the basic geometry given in Fig. 1. There will be some additional copper between the lithium target and the patient, and inlet and outlet cooling lines will be added, but most of the volume between the target and phantom is still H_2O. This small reduction in the hydrogen atom density will change the advantage parameters slightly, but the gross variations of RBE-AD, RBE-AR, and RBE-ADDR with parameters such as proton beam energy and moderator thickness will only change by a few percent. This has been demonstrated elsewhere.[29]

VI. COMPARISON WITH OTHER ACCELERATOR BNCT DESIGNS

As a result of this systematic study, the following set of design parameters has been determined which meet the minimum therapeutic criteria stated in Sec. II:

- Proton energy: 1.95 MeV
- Target: 9.5 μm natural Li
- Target backing: 0.25 cm Cu
- Moderator: 5 cm H_2O
- Thermal neutron shield: 0.01 cm ^{6}Li
- Photon shield: 0.25 cm Pb

It is instructive to compare the treatment figures of merit determined in this work with other accelerator-based BNCT designs. The designs of Yanch, Zhou, Shefer, and Klinkowstein (YZSK)[7] and Woollard, Blue, Gupta, and Gahbauer (WBGG)[6] will be considered here. Comparisons will require modeling of the CTU configurations given in these papers, since the WBGG design analysis does not use the same figures of merit used here, while the YZSK design analysis uses older RBE values and boron concentrations.

The YZSK design uses a heavy water (D_2O) moderator and Pb reflector, with a D_2O/^{6}Li neutron shield surrounding

TABLE III. Comparison of accelerator-based BNCT neutron sources.

Design	RBE-AD (cm)	RBE-AR	RBE-ADDR (RBE-cGy/mA-min)	5 mA treatment time (minutes)	Total CTU mass (kg)
YZSK	8.5	4.1	7.9	32	1258
WBGG	9.2	5.0	1.3	190	874
Near-threshold (1.95 MeV)	5.9	4.8	7.1	35	159

the reflector. The moderator used in this comparison has a 12 cm radius and 19 cm thickness. The 2.5 MeV proton beam is uniform over a 4 cm diameter circular area. The ^{6}Li thickness at the moderator exit, as well as surrounding the D_2O shield, is 0.01 cm.

The WBGG design uses a BeO moderator and Li_2CO_3 reflector. The multiple sections of the CTU are separated by thin (0.5 cm) layers of a magnesium/aluminum alloy. The front of the CTU has an annulus of D_2O for neutron shielding, and the moderator surface and D_2O shield are coated with a thin (0.01 cm) layer of ^{6}Li. The patient head is placed inside the inner radius of the D_2O shield. The moderator used in this comparison has a 15.5 cm radius and 20 cm thickness. The 2.5 MeV proton beam is uniform over a 13 cm radius circular area, nominally designed for a 10 mA accelerator current.

The YZSK and WBGG designs were modeled using the same head phantom, material compositions, boron concentrations, and RBE values used in the near-threshold analyses discussed previously. The three designs are compared in Table III. Note that the figures of merit for the YZSK design presented here differ from those in their paper for the reasons given above.

Each design clearly has advantages and disadvantages. The YZSK and WBGG designs have superior RBE-ADs, and therefore can treat deeper tumor systems than the near-threshold design. The near-threshold RBE advantage ratio is greater than the YZSK design and less than the WBGG design, although all three are comparable. The YZSK design RBE-ADDR is slightly greater than the near-threshold value, indicating a slightly shorter treatment time for equal accelerator currents, while the WBGG design RBE-ADDR is roughly five times lower. This is due to the larger source area, which provides a more uniform beam exiting the CTU at the expense of longer treatment times or higher accelerator currents. The total CTU mass of the near-threshold design is 5.5 times smaller than the WBGG system mass and 7.9 times smaller than the YZSK system mass.

Another advantage to near-threshold BNCT relative to higher proton energies will be the lower induced radioactivity in the lithium target. Each (p,n) reaction will produce both a neutron and a radioactive ^{7}Be nucleus, which decays with a 53.3 day half-life via electron capture followed by emission of a 478 keV gamma 10.4% of the time.[31] The ^{7}Be production rates per unit proton current are equivalent to the neutron yields in the second column of Table I; for 1.95 MeV and 2.5 MeV proton beams, these production rates may be written as 1.68 and 23.9 Ci/mA, respectively. Approximating the target as a point source (a good approximation for the near-threshold and YZSK designs), the exposure rate in air is given by $\dot{D}=\Gamma A_\gamma/d^2$, where Γ is the specific gamma ray emission, A_γ is the ^{7}Be activity, and d is the distance from the target.[32] For ^{7}Be, Γ is 24.8 mR-m^2/Ci-h.

Assuming four BNCT treatments are performed each day of a 5-day work week, then using the treatment times given in Table III, the total amount of time that 1.95 MeV (near-threshold) and 2.5 MeV (YZSK design) proton beams are turned on each week will be 11.7 and 10.7 h, respectively. Since these times are much shorter than the ^{7}Be half-life, the buildup of activity increases approximately linearly with time, and the exposure rates in air one meter from the target at the end of the week are 1.32 and 17.1 mR/h, respectively, for a 5 mA accelerator current. Higher weekly accelerator workloads (in mA-min) will produce correspondingly higher exposure rates for the bare target. The 478 keV photon source from ^{7}Be decays will not affect the advantage parameters already calculated for these designs, but any maintenance that requires the CTU to be removed from the beamline can lead to significant exposure rates for workers. While the exposure rates after one week that are given above are not restrictively high, they will not decay appreciably for many months, so that lithium targets that are not exchanged regularly will provide increasingly high exposure rates when the CTU is removed.

VII. SUMMARY

A systematic study of the near-threshold neutron source concept for BNCT has been performed using quantitative figures of merit based on head phantom dosimetry calculations. This has led to a BNCT neutron source design capable of treating tumors located within 5.9 cm of the head surface in less than 35 minutes using a 5 mA proton accelerator. The specifics of this design were given in the previous section. The design proton energy is part of an envelope of acceptable energies, ranging from 1.93 to 1.99 MeV. 1.91 MeV proton beams can also produce acceptable BNCT treatment beams if no ^{6}Li and lead are added to the CTU; adding these materials drops the RBE-ADDR below the acceptability criterion.

Note that the penetrability (RBE-AD) of near-threshold beams may be increased to values greater than 7 cm using greater thicknesses of moderator, ^{6}Li, and lead, but the concomitant decrease in dose rate (RBE-ADDR) pushes treatment times and/or accelerator currents higher than the 1 hour and 5 mA restrictions, respectively, used in this research. Neutron beams with greater penetrabilities, such as reactors or the accelerator designs discussed in Sec. VI, are available for deeply seated tumors. For more shallow tumors, near-threshold beams provide an attractive, lightweight, and relatively low cost alternative neutron source for hospital-based BNCT.

Accelerator costs depend strongly on beam current capacity, so that the lower currents used by near-threshold beams

and the YZSK design indicate an economic advantage over the WBGG design. For certain types of accelerators, a lower beam energy can also reduce the system cost relative to a higher beam energy. This indicates another potential economic advantage to near-threshold beams over higher proton energy beams such as the YZSK and WBGG designs. These lower costs may allow smaller hospitals with less capital money at their disposal to have the opportunity to participate in neutron-based treatments such as BNCT.

All the CTU masses given in Table III may be mounted on standard isocentric gantries already in widespread use for conventional hospital-based radiotherapy, allowing greater flexibility in patient treatment planning with accelerator-based BNCT than with reactor beams. However, routine hospital use will require regular changing of the target to prevent excessive buildup of ^{7}Be activity in the lithium, as described in Sec. VI. The much lower mass of the near-threshold CTU is expected to make regular target exchange simpler than with either the YZSK or WBGG design.

The final CTU design requires detailed modeling of a target cooling system, but all the design parameters described here should not change appreciably with the more detailed model. Additional MCNP dosimetry calculations have begun to determine a final set of RBE-AD, RBE-AR, and RBE-ADDR values for this near-threshold beam design.

Further work will involve incorporating the final near-threshold beam into treatment planning software that provides more detailed models of human heads and tumor systems. Direct comparison with existing reactor beams, as well as other accelerator-based beams, will be made using dose–volume histograms and tumor control probabilities. In addition, an evaluation of the utility of near-threshold beams for other applications related to BNCT, such as the treatment of rheumatoid arthritis, is underway.

[a]Current address: X-11, MS F663, Los Alamos National Laboratory, Los Alamos, New Mexico 87545.

[1] A. H. Soloway, R. F. Barth, R. A. Gahbauer, T. E. Blue, and J. H. Goodman, ''The rationale and requirements for the development of boron neutron capture therapy of brain tumors,'' J. Neuro-Oncol. **33**, 9–18 (1997).

[2] Y. Mishima *et al.*, ''Selective melanoma thermal neutron capture therapy for lymph node metastases,'' *Advances in Neutron Capture Therapy*, edited by A. H. Soloway, R. F. Barth, and D. E. Carpenter (Plenum, New York, 1993), 705–710.

[3] E. Binello, R. E. Shefer, and J. C. Yanch, ''Neutron beam design for boron neutron capture synovectomy,'' *Advances in Neutron Capture Therapy: Volume I, Medicine and Physics*, edited by B. Larsson, J. Crawford, and R. Weinreich (Elsevier, Amsterdam, 1997).

[4] J. C. Yanch, X.-L. Zhou, and G. L. Brownell, ''A Monte Carlo investigation of the dosimetric properties of monoenergetic neutron beams for neutron capture therapy,'' Radiat. Res. **126**, 1–20 (1991).

[5] J. H. Gibbons and R. L. Macklin, ''Total neutron yields from light elements under proton and alpha bombardment,'' Phys. Rev. **114**, 571–580 (1959).

[6] J. E. Woollard, T. E. Blue, N. Gupta, and R. A. Gahbauer, ''Evaluation of moderator assemblies for use in an accelerator-based neutron source for boron neutron capture therapy,'' Nucl. Technol. **123**, 320–333 (1998).

[7] J. C. Yanch, X.-L. Zhou, R. E. Shefer, and R. E. Klinkowstein, ''Accelerator-based epithermal neutron beam design for neutron capture therapy,'' Med. Phys. **19**, 709–721 (1992).

[8] D. A. Allen and T. D. Beynon, ''A design study for an accelerator-based epithermal neutron beam for BNCT,'' Phys. Med. Biol. **40**, 807–821 (1995).

[9] R. J. Kudchadker, J. F. Kunze, and J. F. Harmon, ''Balancing neutron yield and moderator dimensions in accelerator neutron sources,'' in Ref. 3.

[10] J. F. Harmon, R. J. Kudchadker, J. F. Kunze, S. W. Serrano, X. L. Zhou, Y. D. Harker, and R. W. Hamm, ''Accelerator neutron sources for neutron capture therapy using near threshold charged particle reactions,'' *Proceedings of the 14th International Conference on the Application of Accelerators in Research and Industry*, edited by J. L. Duggan and I. L. Morgan (AIP, Woodbury, NY, 1997).

[11] X.-L. Zhou, C. Lee, F. Harmon, Y. Harker, and R. Hamm, ''Analysis of epithermal neutron production by near-threshold (p,n) reactions,'' Appl. Radiat. Isot. **48**, 1571–1575 (1997).

[12] R. J. Kudchadker, ''Optimized accelerator based epithermal neutron beams for boron neutron capture therapy,'' Ph.D. dissertation, University of Missouri—Columbia, 1996.

[13] R. L. Moss, O. Aizawa, D. Beynon, R. Brugger, G. Constantine, O. Harling, H. B. Liu, and P. Watkins, ''The requirements and development of neutron beams for neutron capture therapy of brain cancer,'' J. Neuro-Oncol. **33**, 27–40 (1997).

[14] D. A. Allen, T. D. Beynon, and S. Green, ''Design for an accelerator-based orthogonal epithermal neutron beam for neutron capture therapy,'' Med. Phys. **26**, 71–76 (1999).

[15] R. G. Zamenhof, B. W. Murray, G. L. Brownell, G. R. Wellum, and E. I. Tolpin, ''Boron neutron capture therapy for the treatment of cerebral gliomas. I: Theoretical evaluation of the efficacy of various neutron beams,'' Med. Phys. **2**, 47–60 (1975).

[16] R. Zamenhof, E. Redmond II, G. Solares, D. Katz, K. Riley, S. Kiger, and O. Harling, ''Monte Carlo-based treatment planning for boron neutron capture therapy using custom designed models automatically generated from CT data,'' Int. J. Radiat. Oncol., Biol., Phys. **35**, 383–397 (1996).

[17] J. A. Coderre, M. S. Makar, P. L. Micca, M. M. Nawrocky, H. B. Liu, D. D. Joel, D. N. Slatkin, and H. I. Amols, ''Derivations of relative biological effectiveness for the high-LET radiations produced during boron neutron capture irradiations of the 9L rat gliosarcoma *in vitro* and *in vivo*,'' Int. J. Radiat. Oncol., Biol., Phys. **27**, 1121–1129 (1993).

[18] J. F. Briesmeister, ''MCNP—A general Monte Carlo N-Particle Transport Code, version 4A,'' LA-12625-M, Los Alamos National Laboratory, 1993.

[19] C. L. Lee and X.-L. Zhou, ''Thick target neutron yields for the ^{7}Li$(p,n)^{7}$Be reaction near threshold,'' Nucl. Instrum. Methods Phys. Res. B **152**, 1–11 (1999).

[20] C. L. Lee and X.-L. Zhou, ''An algorithm for computing thick target differential *p*-Li yields near threshold,'' *Proceedings of the 15th International Conference on the Application of Accelerators in Research and Industry*, edited by J. L. Duggan and I. L. Morgan (AIP, Woodbury, New York, 1999).

[21] R. Brooks, G. DiChiro, and M. R. Keller, ''Explanation of cerebral white-gray contrast in computed tomography,'' J. Comput. Assist. Tomogr. **4**, 489–491 (1980).

[22] R. S. Caswell, J. J. Coyne, and M. L. Randolph, ''Kerma factors of elements and compounds for neutron energies below 30 MeV,'' Int. J. Appl. Radiat. Isot. **33**, 1227–1262 (1982).

[23] A. Z. Kiss, E. Koltay, B. Nyako, E. Somorjai, A. Anttila, and J. Raisanen, ''Measurements of relative thick target yields for PIGE analysis on light elements in the proton energy interval 2.4–4.2 MeV,'' J. Radioanal. Nucl. Chem. **89**, 123–141 (1985).

[24] J. F. Janni, ''Proton range-energy tables, 1 keV–10 GeV,'' At. Data Nucl. Data Tables **27**, 147–339 (1982).

[25] C. L. Lee, X.-L. Zhou, R. W. Hamm, F. Harmon, R. J. Kudchadker, and Y. D. Harker, ''Temperature rise in lithium targets for accelerator based BNCT using multi-fin heat removal,'' in Ref. 20 (AIP, Woodbury, New York, 1999).

[26] W. E. Sweeney, Jr. and J. B. Marion, ''Gamma-ray transitions involving isobaric-spin mixed states in Be^{8},'' Phys. Rev. **182**, 1007–1021 (1969).

[27] O. K. Harling, K. A. Roberts, D. J. Moulin, and R. D. Rogus, ''Head phantoms for neutron capture therapy,'' Med. Phys. **22**, 579–583 (1995).

[28] M. C. Dobelbower and T. E. Blue, ''A Monte Carlo analysis of the effect of increasing target diameter for an accelerator-based neutron source for

BNCT,'' *Proceedings of the American Nuclear Society Embedded Topical Meeting on Nuclear Applications of Accelerator Technology*, Albuquerque, NM, 1997, pp. 495–501.
[29] C. L. Lee, ''The design of an intense accelerator-based epithermal neutron beam prototype for BNCT using near-threshold reactions,'' Ph.D. dissertation, Massachusetts Institute of Technology, 1998.
[30] M. C. Dobelbower, T. E. Blue, and K. Vafai, ''Effect of duty factor and repetition rate on maximum target temperature for a proposed BNCT target assembly,'' in Ref. 28.
[31] D. R. Lide, in *Table of Isotopes*, 78th ed. (CRC, New York, 1997–1998).
[32] H. Cember, *Introduction to Health Physics*, 2nd ed. (Pergamon, New York, 1985).